

SUPPORTING INFORMATION

$\text{Li}_9\text{V}_3(\text{P}_2\text{O}_7)_3(\text{PO}_4)_2$ nanotubes fabricated by a simple molten salt approach with excellent cycling stability and enhanced rate capability for lithium-ion batteries

Xue Miao, ^{a,b} Chun Li, ^{a,b} Wei Chu, ^{c*} Ping Wu ^{a,b} and Dong Ge Tong ^{a,b*}

^a Mineral Resources Chemistry Key Laboratory of Sichuan Higher Education Institutions, College of Materials and Chemistry & Chemical Engineering, Chengdu University of Technology, Chengdu 610059, China. E-mail: tongdongge@163.com; Fax: +86 28 8407 9074

^b State Key Laboratory of Oil and Gas Reservoir Geology and Exploitation, Chengdu University of Technology, Chengdu 610059, China

^c College of Chemical Engineering, Sichuan University, Chengdu 610065, China.

E-mail: chuwei1965@foxmail.com; Fax: +86 28 8540 3397

Summary: 8 Pages; 7 Figures;

Experimental

Synthesis of $\text{Li}_9\text{V}_3(\text{P}_2\text{O}_7)_3(\text{PO}_4)_2$ nanotubes

All the reagents were analytical grade and without further purification before utilization. The molten salt reactor (Chanzheng AMS-70, China) was run using a personal computer through reaction conditions (time and temperature, etc.) control software. In a typical synthesis, a mixture of LiH_2PO_4 and NaNO_3 (weight ratio of LiH_2PO_4 : $\text{NaNO}_3=1:2$) was firstly heated to 580 °C to form the molten salt in the reactor under Ar. Into it VCl_2 was added under stirring (the weight percentage of VCl_2 in the reaction system was about 8.5 %). After the reaction was conducted for 10 min, and then cooling to room temperature, the product was obtained by washing the fusion with deionized water to remove the nitrates for several times, and dried in 100 °C for 12 h.

Characterization of $\text{Li}_9\text{V}_3(\text{P}_2\text{O}_7)_3(\text{PO}_4)_2$ nanotubes

X-ray diffraction (XRD) patterns were obtained using an X'Pert X-ray powder diffractometer equipped with a $\text{CuK}\alpha$ radiation source ($\lambda = 0.15406$ nm). For compositional analyses, the dry samples were dissolved in boiling aqua fortis using a microwave digestion system. The Brunauer–Emmett–Teller (BET) specific surface areas of the samples were determined using a N_2 adsorption–desorption technique, in which the samples were degassed at 200 °C for 180 min before the measurements. Scanning transmission electron microscopy (STEM) images and selected-area electron diffraction patterns (SAED) of the samples were taken using a FEI Tecnai G2 F20 S-Twin microscope. Samples for STEM analysis were prepared by depositing a single drop of diluted nanoparticle dispersion in ethanol on an amorphous, carbon-coated, copper grid. The energy dispersive X-ray spectroscopy (EDAX) data were acquired using an Oxford

Instrument EDAX detector. The measured compositions were typically averaged from 5–10 spots, with an estimated systematic error of less than ± 2 at.%. The surface electronic states of the samples were investigated using X-ray photoelectron spectroscopy (XPS; Perkin–Elmer PHI 5000C ESCA, using $AlK\alpha$ radiation). The binding energies were referenced to the C1s peak (binding energy of 284.6 eV) of the surface adventitious carbon. Infrared spectra were acquired using a Bruker FTIR spectrometer (EQUINOX55).

Electrochemical performances were evaluated using a CR2032 coin cell composed of the cathode, lithium anode, Celgrade polypropylene separator, and $LiPF_6$ in 1:1 ethylene carbonate and diethyl carbonate as the electrolyte. The cathode was prepared by mixing the samples with 20 wt.% acetylene black and 15 wt.% polytetrafluoroethylene binder. The cells were galvanostatically cycled at different current rates ($1\ C=170\ mA\ g^{-1}$) in the range 2.5–4.6 V using an Arbin Instruments testing system (Arbin BT-2000).

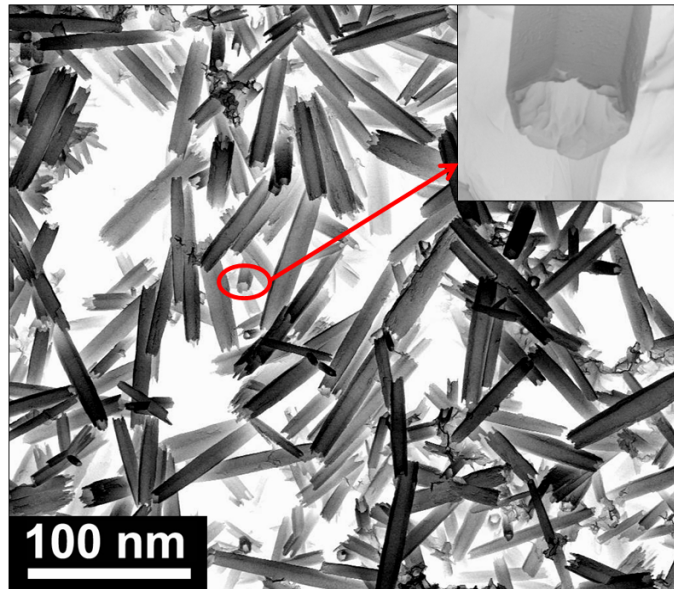


Fig.S1 Typical STEM images of $\text{Li}_9\text{V}_3(\text{P}_2\text{O}_7)_3(\text{PO}_4)_2$ nanotubes after sonication for 2 h dispersed in ethanol.

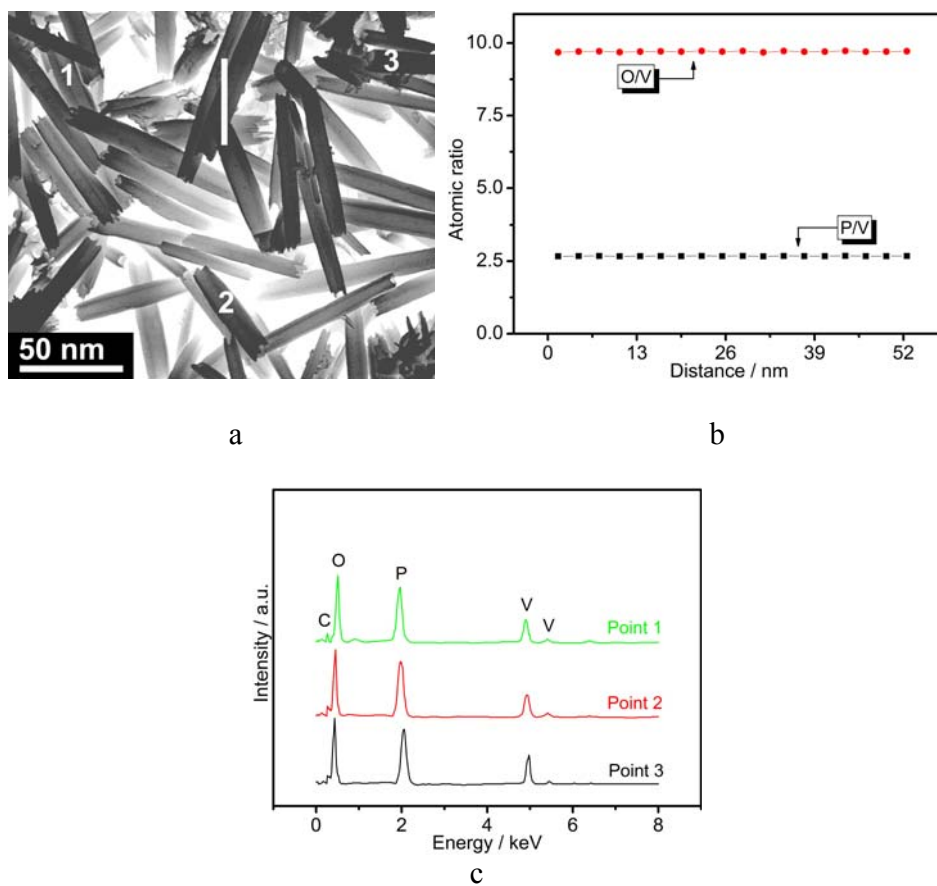


Fig.S2 (a) The high-angle annular dark-field scanning transmission electron microscopy (HAADF-STEM); (b) P/V and O/V atomic ratios recorded along the white cross-sectional compositional line shown in (a); (c) the Energy-dispersive X-ray spectroscopy (EDS) at points 1-3 in (a) of the as-prepared $\text{Li}_9\text{V}_3(\text{P}_2\text{O}_7)_3(\text{PO}_4)_2$ nanotubes.

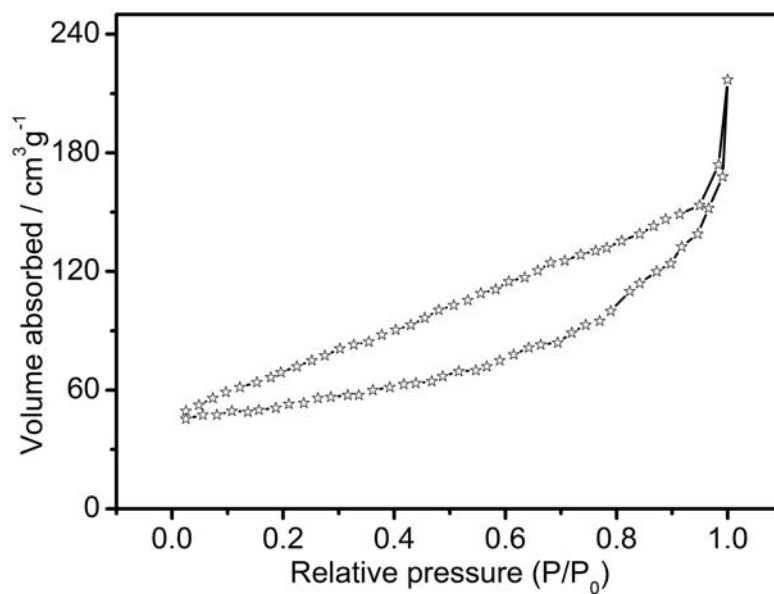


Fig.S3 Nitrogen adsorption-desorption isotherm of the as-prepared $\text{Li}_9\text{V}_3(\text{P}_2\text{O}_7)_3(\text{PO}_4)_2$ nanotubes.

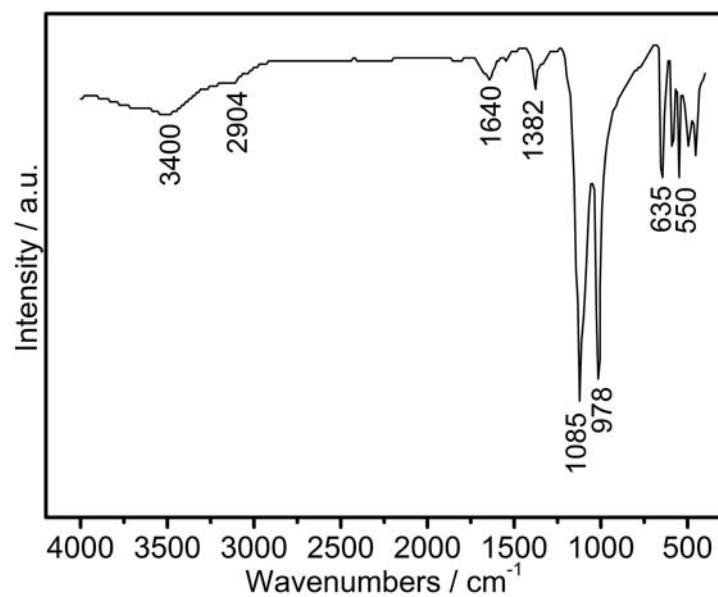


Fig. S4 FT-IR spectrum of the as-prepared $\text{Li}_9\text{V}_3(\text{P}_2\text{O}_7)_3(\text{PO}_4)_2$ nanotubes.

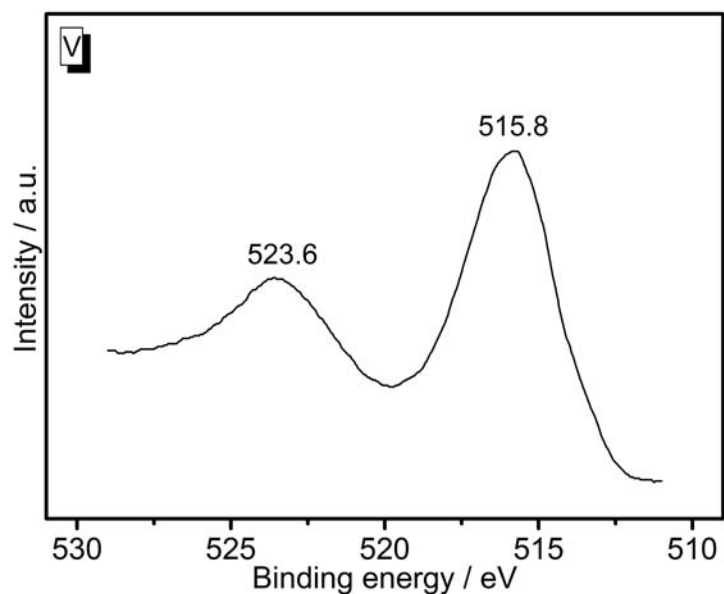


Fig. S5 V 2p XPS spectra in the as-prepared $\text{Li}_9\text{V}_3(\text{P}_2\text{O}_7)_3(\text{PO}_4)_2$ nanotubes.

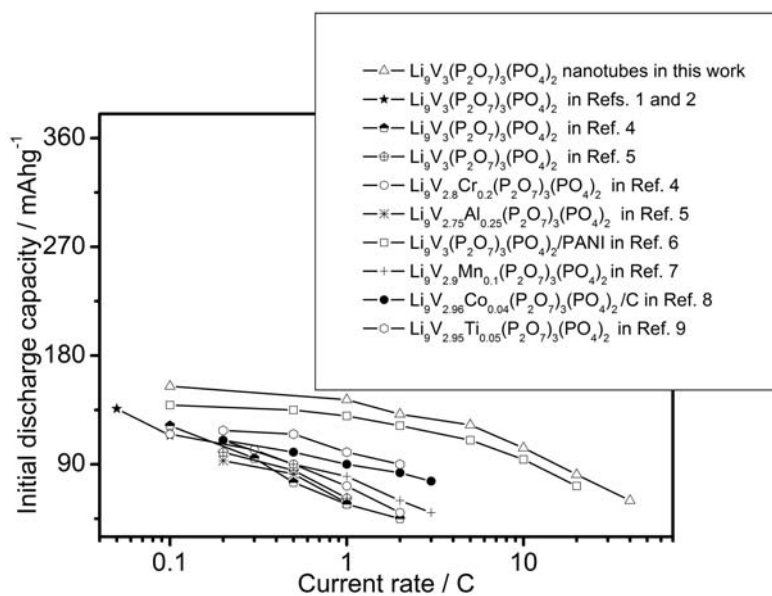


Fig.S6 Rate performance comparison of $\text{Li}_9\text{V}_3(\text{P}_2\text{O}_7)_3(\text{PO}_4)_2$ nanotubes with those previously reported for similar materials.

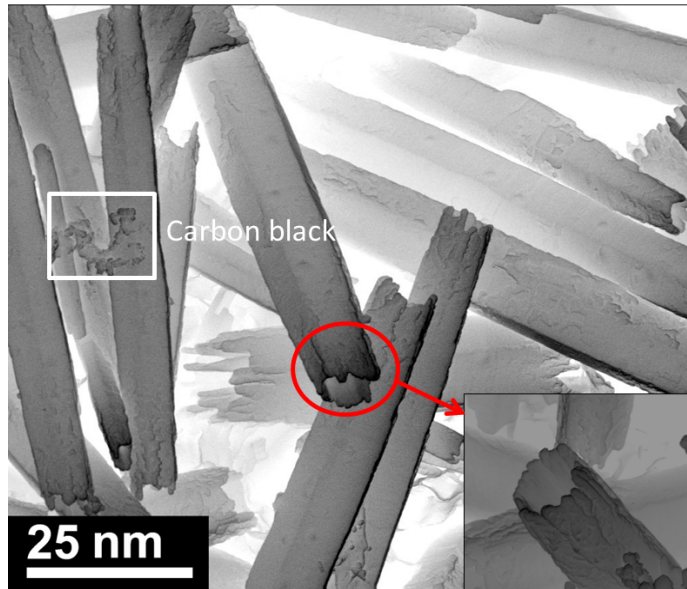


Fig.S7 STEM images of $\text{Li}_9\text{V}_3(\text{P}_2\text{O}_7)_3(\text{PO}_4)_2$ nanotubes after cycling at 5 C for 100 cycles. The small nanoparticles observed in the images are carbon black.